Development of Highly Photoactive Mixed Metal Oxide (MMO) Based on The Thermal Decomposition Of ZnAl-NO3-LDH

Humaira Asghar * , Valter Maurino , Muhammad Ahsan Iqbal

Posted Date: 8 March 2024

doi: 10.20944/preprints202403.0534.v1

Keywords: ZnAl-NO3-LDH, Mixed Metal Oxides, Photocatalysis, Calcination, ZnO, Phenol.

Article

Development of Highly Photoactive Mixed Metal Oxide (MMO) Based on the Thermal Decomposition of ZnAl-NO_3-LDH

Humaira Asghar [1,*], Valter Maurino [1,2] and Muhammad Ahsan Iqbal [3]

[1] Department of Chemistry, University of Torino, Via Giuria 7, 10125 Torino, Italy
[2] JointLAB UniTo-ITT Automotive, Via Quarello 15/A, 10135 Torino, Italy
[3] Departamento de Ingeniería Química y de Materiales, Facultad de Ciencias Químicas, Universidad Complutense de Madrid, 28040 Madrid, Spain
* Correspondence: humaira.asghar@unito.it

Abstract: The highly crystalline ZnAl Layered Double Hydroxides (ZnAl-NO_3- LDHs) are utilized for the potential transformation into Mixed Metal oxides (MMO) through thermal decomposition and used further for the photodegradation of phenol to assess the influence of calcination on ZnAl LDHs with enhanced photoactivity. The structure, composition, and morphological evolution of ZnAl-LDHs to ZnO-based MMO nanocomposites, which are composed of ZnO and $ZnAl_2O_4$, after calcination at different temperatures (400-600 ^{o}C), are all thoroughly examined in this work. The final ZnO and $ZnAl_2O_4$ base nanocomposites showed enhanced photocatalytic activity. The findings demonstrated that calcining ZnAl-LDHs from 400 to 600 °C increased the specific surface area and also enhanced the interlayer spacing of d_{003} while the transformation of LDHs into ZnO/$ZnAl_2O_4$ nanocomposite through calcining the ZnAl-LDH precursor at 600 °C showed significant photocatalytic properties, leading to complete mineralization of phenol under UV irradiation.

Keywords: ZnAl-NO_3-LDH; mixed metal oxides; photocatalysis; calcination; ZnO; phenol

1. Introduction

Zinc oxide and titanium dioxide (TiO_2) base nanomaterials are typical metal oxide nanostructures that are proven to be important for photocatalytic applications [1,2]. However, ZnO and TiO_2 are also broad bandgap metal oxides that can be photoexcited only when exposed to UV light [3]. Although bandgap narrowing can be accomplished by increasing the top of the valence band or decreasing the bottom of the conduction band through doping or other methods, remains unsolved issues, related to the mass transfer of the substrates onto the surface and to high rates of photoexcited carriers' recombination. Photocatalysts with large pore volume and surface area are necessary for an effective alternative and efficient treatment [3][4]. Recently, mixed metal oxides have been widely reported for their interesting properties that enhance their catalytic activity [5–10]. Mixed metal-oxide (MMO) photocatalysts, namely heterostructures with two or more metal oxides, can effectively separate photo-induced electron-hole pairs by properly adjusting the band structures, thereby extending the lifetime of electrons and holes in comparison to common photocatalysts (such as ZnO or TiO_2). Among the new generation of heterogeneous photocatalysts, mixed metallic oxides (MMOs), which are developed from layered double hydroxides (LDHs) by controlling the temperature of thermal decomposition, are regarded as possible alternative photocatalytic material because of the enhanced light absorption spectrum and better charge separation-transport capabilities.

The layered double hydroxide (LDHs), also known as anionic clays, are composed of positively charged brucite-like layers and exchangeable anions with chemical formula generally described as $[M^{2+}_{1-x}M^{3+}_{x}\cdot x(OH)_2]A^{n-}_{x/n}\cdot mH_2O]$, where M^{2+} is a divalent metal cation (e.g., Mg^{2+}, Zn^{2+}, Ni^{2+}, Ca^{2+}, etc.), M^{3+} is a trivalent cation (e.g., Al^{3+}, Fe^{3+}, Cr^{3+}, etc.), and A^{n-} is an exchangeable anion such as CO_3^{2-},

 doi:10.20944/preprints202403.0534.v1

NO_3^{1-}, SO_4^{2-}, etc. Due to the variation in metal composition, even ternary or quaternary metal composition is possible along with high anionic exchange capacity, and anisotropic structure [11–14]. Furthermore, eco-friendly LDHs have a "memory effect" that supports material sustainability, which is required for dye degradation [15–18] and other photocatalytic processes. It is also well-known that LDH, upon calcination, undergoes phase transformation to MMO through sequential dehydration, dehydroxylation, and elimination of interlayer anions, wherein various layers are stacked one above another in different fashions and thus can obtain different polytypes with random or ordered stacking [19–21]. Numerous studies have been published where the calcined LDH structure was employed to remediate heavy metal contamination and showed better effectiveness than uncalcined LDH [22] [10]. The use of layered double hydroxides (LDHs) as anion immobilization agents requires knowledge of their stability under the operating conditions in which they are intended to be used, which is dependent on the M^{2+}/M^{3+} ratio used for LDH synthesis and must always be considered to propose a strategy for increasing photocatalytic efficiency while keeping the reconstitution mechanism of LDHs in mind for sustainability purposes. The potential class of ZnAl-NO_3-LDHs can be considered for possible application as a photocatalytic agent. Recently, *Suárez-Quezada et al.* reported the impact of calcined ZnAl-LDHs into ZnO/$Zn6Al_2O_9$ and ZnO/$ZnAl_2O_4$ heterojunctions by the thermal treatment at 400, 500, 600 and 700 °C and utilized for hydrogen production by water splitting reaction[23]. *E.M. Seftel et al.* describe the 93% efficient methyl-orange photo-oxidation by a ZnAl-LDH with the cationic ratio of 5 and calcined at 500 °C [24]. *A. Elhalil et al*. reported the preparation of ZnO-$ZnAl_2O_4$ mixed phases by calcination of Zn-Al-CO_3 LDH precursors for the degradation performance of caffeine in aqueous solution [25]. Similar work was done by *Zhang et al.* where the RhB photodegradation was conducted to conclude the photocatalytic activity of calcined ZnAl-LDHs due to the improved crystal structure and the better separation of photogenerated electron–hole pairs [26]. *Abdullah Ahmed et al*. reported the transformation of ZnAl-NO_3-LDHs into ZnO phase and $ZnAl_2O_4$ spinel and found that the crystallinity of the ZnO phase increased with an increase in calcination temperature (600-1000 °C) so as the photodegradation behaviour [27]. In summary, the literature describes the effect of calcination temperature range and metallic cationic ratio (1-5) on photodegradation behaviour for liquid and gas phase pollutants.

Although there have been reports of relatively high conversion efficiency in the literature, further research is required to determine the temperature range at which ZnAl-LDHs transform into MMO without undergoing spinal shape morphology, as this is the difficult part of reconstructing ZnAl-LDHs (> 600 ºC). The mixed metal oxides formed by the thermal decomposition of LDHs (< 600 °C) can be regenerated into the original layered structure when they are in contact with water or an anionic solution. The purpose of this work is to improve our understanding of the activity of calcined ZnAl-LDH with high crystallinity, which comes from the controlled synthesis of ZnAl-NO_3-LDHs by adjusting the metallic cationic ratio (M^{2+}/M^{3+}) and by the choice of intercalated anions (NO_3). The highly crystalline ZnAl-NO_3-LDH (2:1) is reported in this work and was further thermally decomposed up to 400–600˚C to achieve MMO for potential photocatalytic material. The relationship between calcined LDH structure and the corresponding photochemical properties was also explored, with particular emphasis on the influence of ZnAl-LDH calcined at 600˚C on LDH geometry. The calcination temperature is chosen to allow for the restoration of the LDH structure, making it a sustainable photocatalysis model. The developed MMO layers from ZnAl-LDHs were utilized to optimize the photodegradation of phenol used as a model pollutant, which has not yet been investigated for this class of nanomaterials. Calcinating the ZnAl-LDH will yield nano-dispersed MMO because the cations in the LDH's brucite-like layers are uniformly distributed. The effectiveness of calcination in developing MMOs derived from LDH precursors is carefully examined, providing a reasonable understanding of the utilization of these new classes of photocatalysts.

 doi:10.20944/preprints202403.0534.v1

2. Materials and Methods

2.1. Synthesis of ZnAl-NO_3 LDH

The LDHs are provided by Smallmatek, Lda (Aveiro, Portugal) and processed according to their manufacturing techniques. In brief, 0.5 M $Zn(NO_3)_2 \cdot 6H_2O$ and 0.25 M $Al(NO_3)_3 \cdot 9H_2O$ were gently added to 1.5 M $NaNO_3$ solution under vigorous stirring at room temperature. Adding 2 M NaOH solution maintained a steady pH (pH = 10 ± 0.5) during the process. The production process was carried out in a custom-made stainless-steel pilot-scale reactor (BTL-Indústrias Metalúrgicas, S.A., Oliveira de Azeméis, Portugal) equipped with a PID (proportional-integral-derivative) controller, which allowed for automatic control and correction of important process parameters (e.g., pH and temperature), and peristaltic pumps for precise chemical addition. The resulting slurry was rinsed with deionized water and filtered under decreased pressure before drying using an industrial spray drier to ensure uniform and fine particles. The powders were then divided into different size fractions using a vibrating sieve shaker (Retsch, Haan, Germany). The synthesized ZnAl-NO_3-LDHs were subsequently calcined at different temperatures (400 ºC, 500 ºC, and 600 ºC) and designated as LDHs-400 ºC, LDH-500 ºC, and LDH-600 ºC, respectively.

2.2. Characterization

The morphology and microstructural characteristics of ZnAl-LDH were analyzed using an SEM (JEOL-IT300 microscope coupled with an EDS detector). The TGA analysis of ZnAl-LDH was obtained by using TA Instruments (TGA Q5000 IR thermobalance (New Castle, DE, USA)) at a heating rate of 10 ˚C/min up to 1000 ˚C under airflow of (10 mL/min), while DSC analysis was studied through Mettler DSC30 calorimeter (Columbus, OH, USA) using 10 mg -LDH powder under airflow of 10 mL/min and up to 600˚C. The XRD patterns of calcined and uncalcined LDH coated samples were recorded by X'Pert High Score diffractometer (Rigaku, Japan) under ambient circumstances utilizing a cobalt K-α (λ=1.54 Å) emission source at 10 mA and 30 kV settings. The step size of 0.005° was modified within a 2θ range of 5-110°. Fourier Transformed Infrared Spectroscopy (FTIR) and an Excalibur Series instrument in the ATR mode were used to analyze the surface functional group and chemical bonding of the samples in the range of 550 to 4000 cm-1 with a 4cm-1 resolution and 32 scans using a diamond crystal as an Internal Reflective element (IRE).

The photocatalytic activity of the catalyst was measured by irradiating suspensions (loading 1 g l-1) in the photoreactor with a fluorescent source with λmax = 365 nm (Philips PL-S 9W BLB, integrated irradiance = 20 W m-2). The photocatalytic activity was calculated as the initial rate of phenol phototransformation by fitting disappearance curves to an exponential decay. An Oceans Optics USB2000 spectrophotometer with a cosine-corrected optical fibre probe was used to measure incident radiant power in the 290-400 nm range. The spectrophotometer was spectroradiometrically calibrated using a NIST traceable DH-2000 CAL UV-Vis source. The starting phenol concentration is 0.1 mM. Measurements were carried out by using ultrapure water as a solvent (pH in the range 5.5-7). To evaluate the pollutant adsorption in the material, the reaction mixture was kept in the dark for 0.5 hours with magnetic stirring. To assess reaction progress, 0.8 mL aliquots of the irradiation solution were sampled at given time intervals using a syringe with a nylon filter (0.45 μm pore size) to separate the suspended photocatalyst particles. The phenol concentration was determined using an Agilent Technologies HPLC chromatograph 1200 Series equipped with a diode array detector, binary gradient high-pressure pump, and an automated sampler. Isocratic elution was performed using a 20/80 acetonitrile/formic acid aqueous solution (0.05% w/v) with a flow rate of 0.5 ml min-1 and an injection volume of 20 μl. The column utilized was a Kinetex C18 150-2 (150 mm length, 2 mm I.D., 2.6 μm core-shell particles, Phenomenex). The detection was carried out at 220 nm.

3. Results and Discussion

The diffractograms of ZnAl-NO_3 of different particle sizes practically overlapped and showed the characteristic reflections peaks of (003), (006), (110), (009), (012) (110) and (113), confirming the formation of well-ordered ZnAl-LDHs [28]. The XRD patterns of the calcined ZnAl-LDHs material

 doi:10.20944/preprints202403.0534.v1

exhibit peaks for the ZnO and $ZnAl_2O_4$ phases. As calcination temperature increases from 400 to 600 °C, ZnO and $ZnAl_2O_4$ particles sharpen and crystallite size increases. The cell unit parameter is defined as a= $2d_{110}$, c= $3d_{003}$= $6d_{006}$=$9d_{009}$, and the thermal treatment caused the reduction of the unit cell parameter with the increase in temperature (up to 500 °C), while further increase transformed the LDHs in ZnO based MMO. The XRD patterns showed that the LDH have the characteristic peaks of LDH during thermal treatment from 400°C -500 °C but caused the contraction of basal spacing that can be attributed to the interlayer water loss, decomposition of the NO_3 group, indicating by the lower interlayer thickness of the LDHs [18,20] [21]. The interlayer spacing d_{003} and d_{006} gradually decreases with the increase of calcination temperature [22]. Calcination at 400 °C causes partial dehydroxylation of the layers and breakdown of interlayer carbonate anions, while over 500°C leads to the development of ZnO and $ZnAl_2O_4$ nanoparticles. As the calcination temperature rises, Zn^{2+} ions are liberated from the amorphous phase, forming crystalline ZnO nanoparticles doped with Al^{3+}. The peak reflections at (003) planes of layered double hydroxide were studied to measure the basal spacing and to define full-width half maximum (FWHM) for the measurement of crystallite size (D) using the Scherrer formula. The cell parameters of ZnAl-LDHs calculated from the XRD pattern are shown in Table 1.

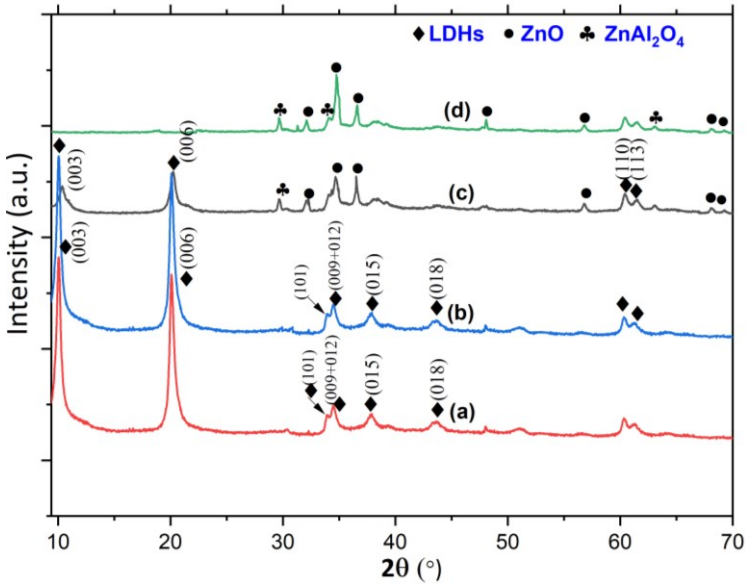

Figure 1. XRD patterns of developed and calcined ZnAl-LDH film samples (a) as-prepared; (b) LDH-400°C (c) LDH-500°C (d) LDH-600°C.

Table 1. Unit-cell parameters of ZnAl-LDHs and Calcined ZnAl-LDHs.

Specimen	Lattice parameter		Interlayer distance			Crystallite size, *D* / nm
	a / nm	*c* / nm	d_{003} / nm	d_{006} / nm	d_{110} / nm	
ZnAl-LDH	0.356	2.71	0.90	19.77	60.322	3.227
LDH-400°C	0.355	2.64	0.88	20.01	60.322	3.147
LDH-500°C	0.355	2.54	0.85	20.12	60.35	3.033

The uncalcined and calcined ZnAl-LDH specimens were further investigated by FT-IR analysis in attenuated total reflection mode, as shown in Figure 3. The broadband displayed in the range of 3370-3427 cm^{-1} assigned to the OH group stretching and absorption band around, 1627 to 1633 cm^{-1} due to the flexural oscillation peaks of interlayer water molecules [24]. Moreover, the absorption peaks around 1350 cm^{-1} are assigned to the asymmetric stretching bond of intercalated NO_3^{-1} [25]. The bonds observed at 655 cm^{-1}, 751 cm^{-1} and 1202 cm^{-1} are associated with the M-OH stretching. The absorption peaks between 550 cm^{-1} to 770 cm^{-1} correspond to the lattice vibration of metal-oxygen bonds (M-O) [29]. Initially, the OH-absorption band receded as the calcination temperature increased. This was followed by a decrease in the NO_3^{1-} absorption peaks, which further indicated the

 doi:10.20944/preprints202403.0534.v1

degradation of anionic species inside the LDH galleries. However, at 600 °C, it was found that there were hardly any absorption peaks of anionic species, which induced the structure of LDH transforming to solely include M-OH and M-O groups (552, 751 cm^{-1}).

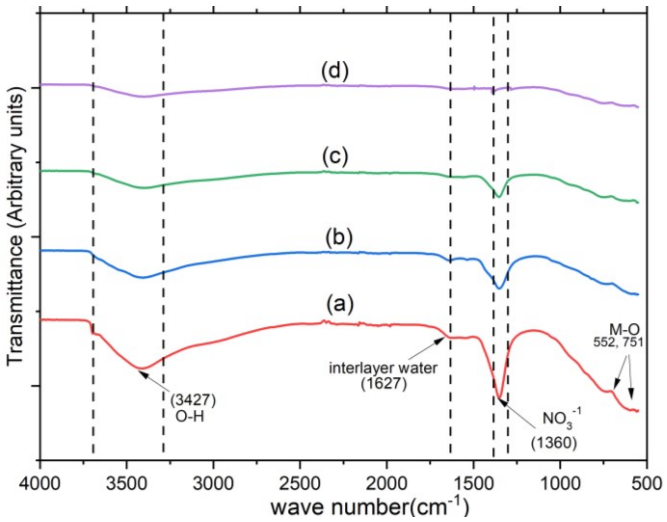

Figure 2. ATR FT-IR spectra of virgin and calcined ZnAl-LDH powder, (a) as-prepared; (b) LDH-400 °C (c) LDH-500 °C (d) LDH-600 °C.

Figure 3 demonstrates the generic concept of utilization of MMO derived from LDHs. The thermal decomposition of ZnAl-LDHs is an indirect construction-reconstruction method in which the mixed oxide obtained after heat treatment of the corresponding LDH can be brought into contact with a solution containing the anion of interest for re-assembly. Upon thermal decomposition, the intensities of the hydroxyl group peaks will decrease, which indicates the loss of the hydroxyl group in the LDH interlayers. Furthermore, peak intensities of the NO_3 group are also reduced, which depicts partial decomposition of the NO_3 group in the interlayer region, especially within the temperature limit of 400 °C. These results suggest that LDH structural decomposition eventuates in two stages: initially, the dehydration of the interlayer water molecules takes place, at around 200°C, while in a later stage, the decomposition of interlayer anions and dehydroxylation is introduced (temperature range 400-600°C) (Figure 4). The obtained findings of this concept are well related to the findings of FT-IR, TGA-DSC, and XRD and with the work done in previous reports [30–32].

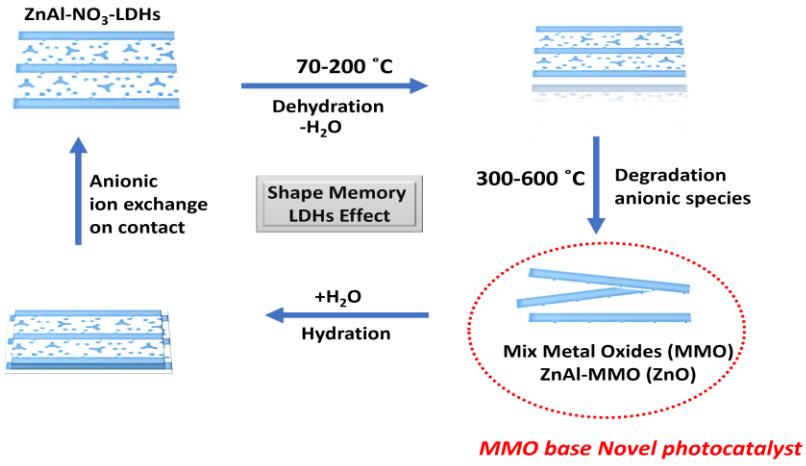

Figure 3. Schematic representation of the memory effect induced ZnAl-LDH structural transformations.

 doi:10.20944/preprints202403.0534.v1

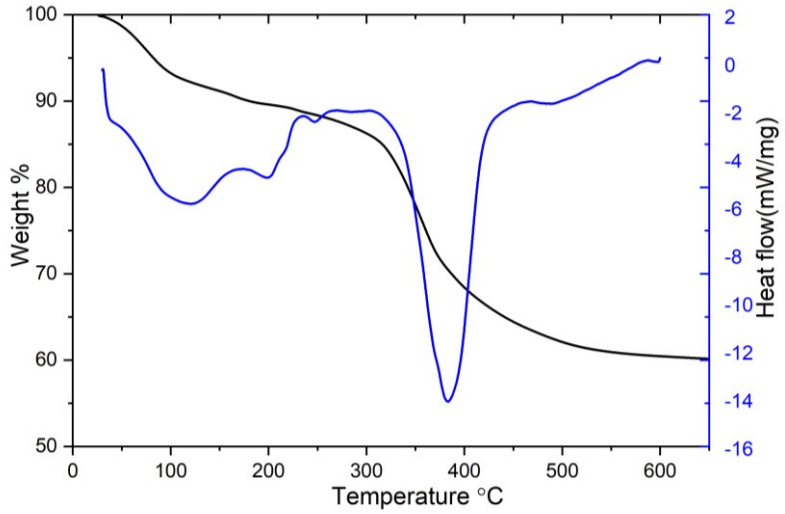

Figure 4. Thermogravimetric analyses of as-prepared ZnAl-NO_3-LDH.

Scanning Electron Microscopy (SEM) was used to investigate the microstructure of uncalcined and calcined ZnAl-LDH. **Figure 5** shows the different macroscopic morphology at 400 and 600 °C, compared to as-prepared ZnAl-LDHs. It is clear from **Figure 5(a)**, that initially a well-developed and distinct nano-platelet-shaped ZnAl-LDH structure is formed which on decomposition the nano-sheets of LDH structure fused to form a spherical flowered structure at 500°C. ZnO nucleation and guided crystal formation may occur during the breakdown of ZnAl-LDH precursors by increasing the calcination temperature to 600°C resulting in the directed development of the ZnO and $ZnAl_2O_4$ phase composition with mixed morphology of distorted nano-belts.

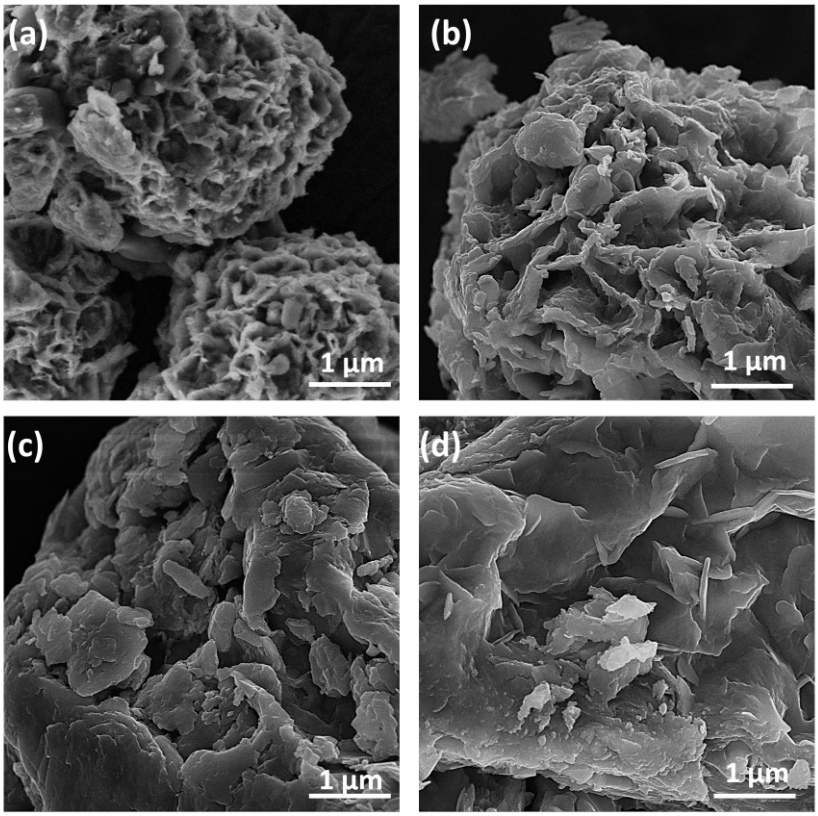

Figure 5. SEM images of uncalcined and calcined ZnAl-LDH films: (a) as-prepared; (b) ZnAl-LDH-400°C; (c) ZnAl-LDH-500°C; (d) ZnAl-LDH-600°C. .

 doi:10.20944/preprints202403.0534.v1

Figure 6 illustrates UV-visible spectra of LDH-600 °C materials specimen where the spectra show how the band gap absorption edges of LDH-600 °C while the large absorption band below 400 nm progressively emerges, indicating that ZnO-based MMO materials may effectively filter UV light. This product effectively absorbs both UVB and UVA rays, comparable to the commercial ZnO [26]. Decomposing the ZnAl-LDH precursor yields a composite material with improved UV-blocking characteristics. The ZnO/$ZnAl_2O_4$ composite material derived from the ZnAl-LDH precursor has a monodisperse particle size distribution and $ZnAl_2O_4$ particles are evenly distributed in the network of ZnO nanoparticles due to the direct decomposition of the LDH. This is due to the high dispersion of the ZnO phase within the amorphous aluminium oxide phase. $ZnAl_2O_4$ is a versatile material that can function as a catalyst, dielectric, optical material, and transparent conductor.

Table 2 displays the computed band gaps of the LDH-600 °C, the band gap of ZnO-based MMO materials reduces, which correlates with a red shift in UV-visible absorption. The band gap of the ZnO/$ZnAl_2O_4$ MMO produced by calcination at 600 °C is 2.98 eV, which is smaller than that of pure ZnO. This might be attributed to the coupling between ZnO and $ZnAl_2O_4$ in the final composite. ZnO-based MMO materials may be tailored for optical and semiconductor characteristics by adjusting their composition and structure through calcination temperature. The ZnAl (2:1) molar ratio is more systematic for thermal decomposition and the derived MMO is more economical than other complicated fabrication methods.

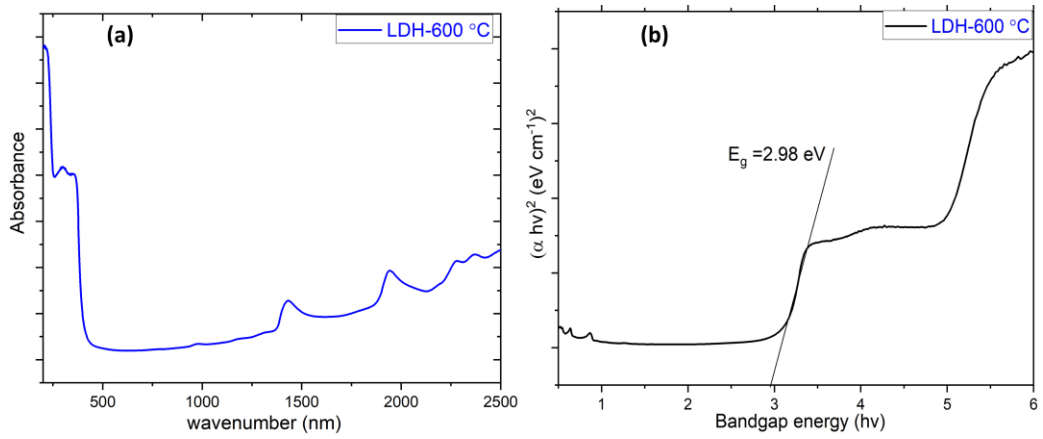

Figure 6. (a) Absorbance spectra, (b) Band gap value determined by UV spectroscopy.

Table 2. BET surface and band gap energy value of developed materials.

	Photon energy (eV)	S_{BET} (m^2g^{-1})
ZnAl-LDH	5.3	44.75
LDH-400°C	4.9	48.09
LDH-500°C	3.9	51.11
LDH-600°C	2.98	71.86

The photocatalytic activity of the developed samples was evaluated by monitoring the oxidative photo-transformation of phenol. A comparison between the degradation curves of these materials (without and with calcination) is shown in **Figure 7**. Modelling of the experimental data (phenol concentration as a function of UV/Vis illumination time) was performed using a pseudo-first-order kinetics model (Langmuir–Hinshelwood model) (Equation (1)):

$$\ln(C/C_0) = -kt \quad (1)$$

 doi:10.20944/preprints202403.0534.v1

where C_0 is an initial concentration, C represents the concentration at time t, and k is the reaction rate constant. The curves show the C/C_0 ratio as a function of the irradiation time. The decays of phenol concentration with time show first-order kinetics for all the samples. This kind of dependence of the concentration on time occurs when the photo-catalytic process is not controlled by the adsorption of the substrate. Data in **Figure 7** were fitted to an exponential decay and the initial disappearance rates of phenol were calculated and reported in **Table 3**. From these results, the photodegradation of phenol involves two stages, the first is the degradation of phenol to intermediate products, while the second involves the mineralization of the intermediate compounds to carbon dioxide and water.

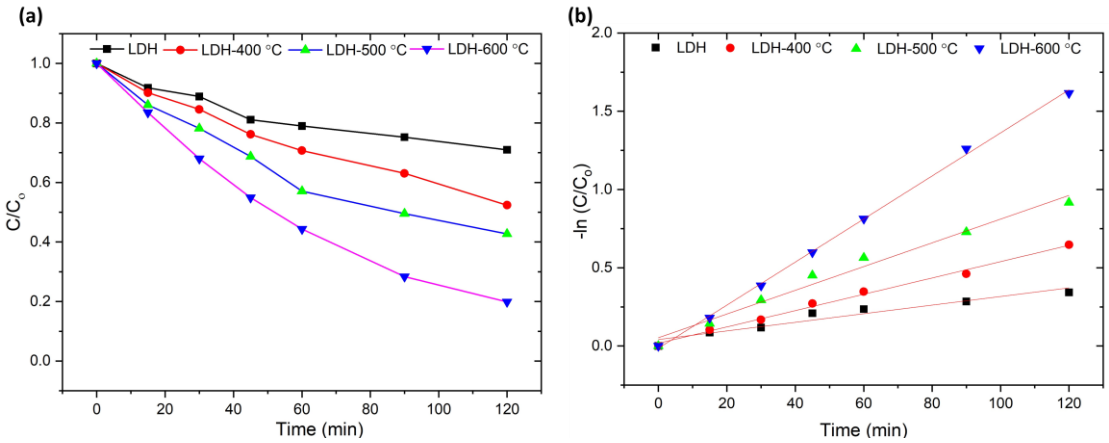

Figure 7. (a) Phenol photodegradation of developed LDHs, (b) Pseudo-first order kinetics plots.

The rate constant of the catalysts increases with increasing calcination temperature, specifically between 400 to 600 ºC. This is because the higher calcination temperature generates more active sites and UV light availability, which improves photocatalytic activity. When the calcined materials were assessed for photocatalytic activity under UV light, it was observed that the degradation of phenol after 120 minutes of irradiation was higher with the material calcined at 600 ºC as compared to the material without calcination. The photocatalytic process in this reaction can be explained as follows: it starts when the calcined photocatalyst is exposed to UV light photons (from an artificial source or sunlight). These photons cause the electrons (e^-) in the valence band to become excited, causing them to rise to the conduction band. When a photon is absorbed in the conduction band (e^- CB), a positive hole is formed in the valence band (h^+ VB) according to Eq. (1). Excited electrons in the conduction band (e- CB) react with the photocatalyst, producing super radicals.

As the calcination temperature increases from 400°C to 600°C, the percentage of phenol abatement also increases from 47% to 80%. The LDH-600°C catalyst is the most effective since it eliminates 80% of phenol with a normalized degradation rate of 0.001268 (mM.min-1). This is well correlated with the XRD and TGA measurements where the developed ZnO and $ZnAl_2O_4$ composite is found to be highly effective for photodegradation. Sensitization of UV and visible light-active materials has gained popularity in recent years as a means of producing photocatalysts with narrower band gaps. In this context, the addition of ZnO and $ZnAl_2O_4$ groups is an attractive option for MMOs which can contribute to the oxidation processes because of their redox potential (E_g = 2.98 eV) with a larger oxidizing ability than $HO^•$ radicals and can be studied further with doping of various nanomaterials for enhanced photodegradation. To pave the road for effective hybrid photocatalytic LDH-based materials, research must be done to find more distinctive morphological structures with increased surface area, superior heterojunction formation, better active sites, and high reactant adsorption. It is also necessary to investigate unique hybrid architectures that have a maximum surface area, improved catalytic sites, and high reactant adsorption. Thus, mixed metal oxides (MMOs) emerge as a new strategy to fully utilize metal oxides as photocatalysts because they retain their unique pristine properties, while further optimization can be obtained by doping different nanomaterials (for selective pollutants degradation), allowing the intrinsic catalytic activity limit to be exceeded in heterostructured MMOs, resulting in higher efficiency.

 doi:10.20944/preprints202403.0534.v1

Table 3. Constant rate (k) and decomposition rate (χ) of phenol in the presence of ZnAl-LDHs based nanomaterials.

	Removal Efficiency	Time			Pseudo-first order Degradation Rate
Material	(%)	(min)	K1 (min-1)	R^2	(mM.min-1)
ZnAl-LDH	20.19	120	0.0033	0.9694	0.000310
LDH-400°C	47.63	120	0.0051	0.9939	0.000471
LDH-500°C	59.17	120	0.0071	0.9951	0.000651
LDH-600°C	80.12	120	0.0136	0.9995	0.001268

4. Conclusion

The calcined ZnAl-LDH structure in this work is found to be highly effective as a photocatalyst, with thermal treatments of ZnAl-LDHs up to 600 °C. This range is feasible given sustainability and recyclability as LDHs can be reconstructed without going to spinal shape morphology. The high crystallinity of synthesized ZnAl-LDHs, due to the feasible M^{2+}/M^{3+} ratio (2:1), is found to be significant for the optimum transformation of LDHs to MMO. The evolution from ZnAl-LDH to $ZnO/ZnAl_2O_4$ composite material has a substantial influence on UV-absorbing and semiconductor properties. Calcination at 500 ºC produced a ZnO phase in a nano-platelet-like structure (hydrotalcite + MMO). As the temperature increased from 500 °C to 600 °C, $ZnAl_2O_4$ nanoparticles developed in the continuous ZnO phase and aggregated between the two phases (ZnO+ $ZnAl_2O_4$). When compared to other calcined ZnAl-LDHs, the composite material containing $ZnAl_2O_4$ demonstrated higher photodegradation efficiencies and a photon energy of 2.8 eV. This work highlighted the utilization of ZnAl-LDHs for the preparation of MMO with relevant photoactivity and sensitization in the violet region of the visible spectrum.

Author Contributions: H. Asghar: Conceptualization, Formal analysis, Methodology, Investigation, Writing - original draft. **M.A Iqbal:** Conceptualization, Formal analysis, Resources, Writing & editing **V. Maurino:** Conceptualization, Formal analysis, Methodology, Writing - original draft, Project administration, Funding acquisition.

Funding: V. Maurino kindly acknowledge funding by Regione Piemonte, Italy, through the project ECOBRAKE "Studio e Sviluppo di materiali frenanti ecologici e a bassa emissione di particolato per applicazioni automotive" – L.R. 34/2004 - D.D. n° 409 del 02/11/2021. M.A Iqbal is grateful for the support of (Marie Skłodowska Curie grant No 847635), the EMULTICOAT European UNA4CAREER project.

Conflicts of Interest: The authors declare no conflict of interest.

References

1. Lin. Yan.; Haiyang. Hu.; Yun. Hang Hu. Role of ZnO morphology in its reduction and photocatalysis. *Appl. Surf. Sci* **2020**, 502, 144202.
2. Kitiyanan. Athapol.; Supachai. Ngamsinlapasathian.; Soropong. Pavasupree.; Susumu. Yoshikawa. The preparation and characterization of nanostructured TiO2–ZrO2 mixed oxide electrode for efficient dye-sensitized solar cells. *J. Solid State Chem* **2005**, 178, 1044-1048.
3. Fan. Guoli.; Wei. Sun.; Hui. Wang.; Feng. Li. Visible-light-induced heterostructured Zn–Al–In mixed metal oxide nanocomposite photocatalysts derived from a single precursor. *J. Chem. Eng* **2011**, 174, 467-474.
4. Mirzaeifard. Zahra.; Zahra. Shariatinia.; Milad. Jourshabani.; Seyed. Mahmood.; Rezaei. Darvishi. ZnO photocatalyst revisited: effective photocatalytic degradation of emerging contaminants using S-doped ZnO nanoparticles under visible light radiation. *Ind. amp; Eng. Chem. Res*. **2020**, 59, 15894-15911.
5. Wachs. Israel. Recent conceptual advances in the catalysis science of mixed metal oxide catalytic materials. *Catal. Today* **2005**, 100, 79-94.
6. Han. Xin.; Yaognag. Li.; Hongzhi. Wang.; Qinghong. Zhang. Controlled preparation of β-Bi 2 O 3/Mg–Al mixed metal oxides composites with enhanced visible light photocatalytic performance. *Res. Chem. Intermed* **2020**, 46, 5009-5021.

 doi:10.20944/preprints202403.0534.v1

7. Zheng. Jiangfu.; Wenbo. Li.; Rongdi. Tang.; Sheng. Xiong.; Daoxin. Gong.; Yaocheng. Deng.; Zhanpeng. Zhou.; Ling. Li.; Long. Su.; Lihua. Yang. Ultrafast photodegradation of nitenpyram by Ag/Ag3PO4/Zn–Al LDH composites activated by persulfate system: removal efficiency, degradation pathway and reaction mechanism. *Chemosphere* **2022**, 292, 133431.
8. Shalaby. Nasser.; M. Sayed. Stover ash-extracted mixed oxides surface-doped with Ni for photo-degradation of water organic pollutants. *Int. J. Environ. Anal* **2023**, 103, 8941-8956.
9. Zheng. Jiangfu.; Changzheng. Fan.; Xiaoming. Li.; Qi. Yang.; Dongbo. Wang.; Abing. Duan.; Jinglin. Ding. Enhanced photodegradation of tetracycline hydrochloride by hexameric AgBr/Zn-Al MMO S-scheme heterojunction photocatalysts: Low metal leaching, degradation mechanism and intermediates. *J. Chem. Eng* **2022**, 446, 137371.
10. Zheng. Jiangfu.; Changzheng. Fan.; Xiaoming. Li.; Qi. Yang.; Dongbo. Wang.; Abing. Duan.; Jinglin. Ding. Enhanced photodegradation of tetracycline hydrochloride by hexameric AgBr/Zn-Al MMO S-scheme heterojunction photocatalysts: Low metal leaching, degradation mechanism and intermediates. *J. Chem. Eng* **2022**, 446, 137371.
11. M. Ahsan. Iqbal.; Michele. Fedel. Effect of operating parameters on the structural growth of ZnAl layered double hydroxide on AA6082 and corresponding corrosion resistance properties. *JCTR* **2019**, 16, 1423.
12. M. Ahsan. Iqbal.; Luyi. Sun.; Allyson T. Barrett.; Michele. Fedel.; Layered double hydroxide protective films developed on aluminum and aluminum alloys: synthetic methods and anti-corrosion mechanisms. *Coatings* **2020**, 10, 428.
13. Yadav. Dileep Kumar.; Sitharaman. Uma.; Rajamani. Nagarajan. Microwave-assisted synthesis of ternary Li-M-Al LDHs (M= Mg, Co, Ni, Cu, Zn, and Cd) and examining their use in phenol oxidation. *Appl. Clay Sci* **2022**, 228, 106655.
14. Liu. Yi.; Tongwen. Yu.; Rui. Cai.; Yanshuo. Li.; Weishen. Yang.; Jürgen. Caro. One-pot synthesis of NiAl–CO 3 LDH anti-corrosion coatings from CO 2-saturated precursors. *RSC Adv* **2015**, 5, 29552.
15. Zhang. Guanhua.; Xueqiang. Zhang.; Yue. Meng.; Guoxiang. Pan.; Zheming. Ni.; Shengjie. Xia. Layered double hydroxides-based photocatalysts and visible-light driven photodegradation of organic pollutants: A review. *J. Chem. Eng* **2020**, 392, 123684.
16. Razzaq. Abdul.; Shahzad. Ali.; Muhammad. Asif.; Su-Il. In. Layered double hydroxide (LDH) based photocatalysts: An outstanding strategy for efficient photocatalytic CO_2 conversion. *Catalysts* **2020**, 10, 1185.
17. Boumeriame. Hanane.; Eliana S. Da Silva.; Alexey. S. Cherevan.; Tarik. Chafik.; Joaquim. L. Faria.; Dominik. Eder. Layered double hydroxide (LDH)-based materials: A mini-review on strategies to improve the performance for photocatalytic water splitting. *J. Energy Chem* **2022**, 64, 406-431.
18. Bian. Xuanang.; Shuai. Zhang.; Yunxuan. Zhao.; Run. Shi.; Tierui. Zhang. Layered double hydroxide-based photocatalytic materials toward renewable solar fuels production. *InfoMat* **2021**, 3, 719-738.
19. Jiménez-López.; R. Leyva-Ramos.; J. Salazar-Rábago.; A. Jacobo-Azuara.; A. Aragón-Piña. Adsorption of selenium (iv) oxoanions on calcined layered double hydroxides of Mg-Al-CO3 from aqueous solution. Effect of calcination and reconstruction of lamellar structure. *Environ. Nanotechnol. Monit. Manag* **2021**, 16, 100580.
20. Wiyantoko. Bayu.; Puji. Kurniawati.; Tri. E. Purbaningtias.; Muhammad. H. Jauhari.; Amri. Yahya.; Muchammad. Tamyiz.; Is. Fatimah.; Ruey-an. Doong. Assessing the effect of calcination on adsorption capability of Mg/Al layer double hydroxides (LDHs). *MRX* **2022**, 9, 035505.
21. Zeng. Bin.; Qingqing. Wang.; Liwu. Mo.; Fei. Jin.; Jun. Zhu.; Mingshu. Tang. Synthesis of Mg-Al LDH and its calcined form with natural materials for efficient Cr (VI) removal. *J. Environ. Chem. Eng* **2022**, 10, 108605.
22. M. Ahsan. Iqbal.; Michele. Fedel. Ordering and disordering of in situ grown MgAl-layered double hydroxide and its effect on the structural and corrosion resistance properties. *Int. J. Miner. Metall* **2019**, 26, 1570.
23. M. G Suárez-Quezada.;., J. Romero-Ortiz.; E. Samaniego-Benítez.; V. Suárez.; A. Mantilla. H_2 production by the water splitting reaction using photocatalysts derived from calcined ZnAl LDH. *Fuel* **2019**, 240, 262.
24. Seftel. E. M.; E. Popovici.; M. Mertens.; K. De Witte.; G. Van Tendeloo.; P. Cool.; E. F. Vansant. Zn–Al layered double hydroxides: Synthesis, characterization and photocatalytic application. *Microporous Mesoporous Mater* **2008**, 113, 296.
25. Elhalil. A.; R. Elmoubarki.; A. Machrouhi.; M. Sadiq.; M. Abdennouri.; S. Qourzal.; N. Barka. Photocatalytic degradation of caffeine by ZnO-ZnAl2O4 nanoparticles derived from LDH structure. *J. Environ. Chem. Eng* **2017**, 5, 3719.
26. Zhang. Zhe.; Zhong. Hua.; Jihui. Lang.; Yuxin. Song.; Qi. Zhang.; Qiang. Han.; Hougang. Fan.; Ming. Gao.; Xiuyan. Li.; Jinghai. Yang. Eco-friendly nanostructured Zn–Al layered double hydroxide photocatalysts with enhanced photocatalytic activity. *CrystEngComm* **2019**, 21, 4607-4619.
27. Ahmed, Ali.; Zainal. Abidin Talib.; Mohd. Zobir bin Hussein.; Azmi. Zakaria. Improvement of the crystallinity and photocatalytic property of zinc oxide as calcination product of Zn–Al layered double hydroxide. *J. Alloys Compd* **2012**, 539, 154.

 doi:10.20944/preprints202403.0534.v1

28. Tedim. J.; S. K. Poznyak.; A. Kuznetsova.; D. Raps.; T. Hack.; M. L. Zheludkevich.; M. G. S. Ferreira. Enhancement of active corrosion protection via combination of inhibitor-loaded nanocontainers. *ACS Appl. Mater. Interfaces* **2010**, 2, 1528.
29. Prevot. V.; C. Forano.; J. P. Besse.; F. Abraham. Syntheses and thermal and chemical behaviors of tartrate and succinate intercalated Zn3Al and Zn2Cr layered double hydroxides. *Inorg. Chem* **1998**, 37, 4293.
30. Mohapatra. Lagnamayee.; Kulamani. Parida. A review on the recent progress, challenges and perspective of layered double hydroxides as promising photocatalysts. *J. Mater. Chem* **2016**, 28, 10744.
31. Ye. Haoyang.; Shiyu. Liu.; Deyou. Yu.; Xuerong. Zhou.; Lei. Qin.; Cui. Lai.; Fanzhi. Qin. Regeneration mechanism, modification strategy, and environment application of layered double hydroxides: Insights based on memory effect. *Chem. Rev* **2022**, 450, 214253.
32. Liu. Jiao.; Peng. Ding.; Zexuan. Zhu.; Wei. Du.; Xiaoyong. Xu.; Jingguo. Hu.; Yong. Zhou.; Haibo. Zeng. Engineering self-reconstruction via flexible components in layered double hydroxides for superior-evolving performance. *Small* **2021**, 17, 2101671.